Submitted, accepted and published by
Fuel Processing Technology, 2012, 96, 37-47

Testing of a highly reactive impregnated Fe_2O_3/Al_2O_3 oxygen carrier for a SR-CLC system in a continuous CLC unit

Pilar Gayán*, Miguel A. Pans, María Ortiz, Alberto Abad, Luis F. de Diego, Francisco García-Labiano, and Juan Adánez

Department of Energy and Environment, Instituto de Carboquímica (C.S.I.C.)

Miguel Luesma Castán 4, 50018 Zaragoza, Spain

Phone number: +34 976 733 977

Fax number: +34 976 733 318

E-mail: pgayan@icb.csic.es

*Corresponding Author. Tel.: +34-976-733977; fax: +34-976-733318;

E-mail address: pgayan@icb.csic.es (P.Gayan)

1. Abstract

A Fe-based oxygen carrier was evaluated for H_2 production with CO_2 capture by coupling steam reforming of methane and chemical–looping combustion processes (SR-CLC). In this process hydrogen is obtained by conventional steam reforming of methane (SR), and the heat necessary to carry out the endothermic reformed reactions is supplied by a chemical-looping combustion (CLC) system with inherent CO_2 capture The tail gas from the PSA unit, a mixture of CH_4, H_2, CO and CO_2, is used as fuel in the CLC system.

The Fe-based oxygen carrier was made by incipient hot impregnation using Al_2O_3 as support and was first characterized by TGA and batch fluidized bed reactor in order to determine the reactivity for CH_4, CO and H_2 and the fluidization behaviour. The oxygen carrier behaviour with respect to gas combustion was evaluated in a continuous CLC unit using a simulated PSA off-gas stream as fuel. Methane was also used as fuel for

comparison purposes. During 46 h of continuous operation, the OC never showed agglomeration problems or carbon deposition, and the loss of fines due to attrition was moderate. It was found that the fuel composition has low effect on the combustion efficiency and full conversion can be obtained at 880ºC with an oxygen carrier-to-fuel ratio > 1.5. The solids inventory needed to fully convert methane or PSA-offgas was found to be lower than those found with other Fe-based materials, both natural and synthetic. These results were due to the important positive effect of using alumina as support for impregnated Fe-based OC on the oxygen carrier reactivity. Therefore, the Fe_2O_3/Al_2O_3 oxygen carrier prepared by impregnation is suitable for burning a PSA tail gas for the H_2 production with CO_2 capture in the SR-CLC process.

Keywords: Hydrogen, Steam Reforming, Chemical Looping Combustion, CO_2 Capture, Oxygen Carrier, Iron oxide, PSA

2. Introduction

It's widely accepted that nowadays there is a global warming due to the increase of greenhouse effect, as a result of the anthropogenic emissions to the atmosphere of greenhouse gases. The main responsible gas is carbon dioxide, coming mostly from fossil fuel combustion. Among the different options to solve the problem, CO_2 capture and storage is a mid-term solution to stabilize the atmospheric CO_2 concentrations [1].

These technologies, currently under development, are easy to apply in power plants, but not in transport sector. The use of H_2 as fuel is a possible option to reduce the CO_2 emissions in vehicles. However, H_2 is an energy carrier that must be produced from a primary energy source. The most widely used technology to obtain hydrogen is steam reforming (SR) [2]. The reforming reaction takes place in the reformer tubes packed with a Ni catalyst. However in the process there are CO_2 emissions generated as a result of the gas combustion necessary to supply enthalpy for the endothermic reforming

reactions. Therefore, to use hydrogen as fuel in vehicles, it would be desirable to find a clean way to produce it, without emitting CO_2 into the atmosphere.

Different Chemical-Looping technologies for the H_2 production coupled with CO_2 capture have been proposed [3-4]. In the chemical-looping reforming (CLR) technology the autothermal reforming of methane is carried out in a chemical looping system [3]. In the SR-CLC technology the H_2 production by steam reforming (SR) coupled with CO_2 capture by chemical-looping combustion (CLC) is accomplished [4]. This process uses the benefits of CLC regarding the CO_2 capture by integrating a CLC unit with the widely used catalytic steam reforming process for H_2 production [2].

CLC is a promising novel combustion technology for CO_2 capture [5]. CLC involves combustion of fuels with an oxygen carrier (OC), generally a metal oxide and a binder, which transfers oxygen from the air to the fuel by means of its circulation between two different fluidized bed reactors, avoiding in this way the direct contact between fuel and air. In conventional combustion the flue gas stream consists of carbon dioxide, steam and mostly nitrogen. Carbon capture in this combustion involves considerable energy penalty for CO_2 separation from N_2. In CLC, CO_2 separation is simply accomplished because the flue gas stream consists only of CO_2 and steam. By steam condensation, a pure CO_2 stream are produced. Therefore, CLC provides a sequestration ready CO_2 stream without the need for using costly gas separation techniques. Moreover, the net chemical reaction and energy release is similar to that of conventional combustion of the fuel.

CLC system is generally composed of two interconnected fluidized bed reactors (Figure 1(a)) designated as air (AR) and fuel reactors (FR), where the solid metal oxide particles are circulated between the reactors. In the fuel reactor, the fuel gas (C_nH_{2m}) is oxidized to CO_2 and H_2O by a metal oxide (MeO) that is reduced to a metal (Me) or a reduced

form of MeO. The FR is typically a bubbling or circulating bed. The metal or reduced oxide is further transferred into the air reactor where it is oxidized with air, and the material regenerated is ready to start a new cycle. The flue gas leaving the air reactor contains N_2 and unreacted O_2. The exit gas from the fuel reactor contains only CO_2 and H_2O.

SR-CLC is a process where steam and hydrocarbons are converted into syngas using reformer tubes packed with catalyst, just as in a conventional tubular steam reforming unit. Figure 1(b) shows the schematic diagram of this process. The main difference with respect to conventional steam reforming is that a CLC system is used as means to provide heat for the endothermic reforming reactions and to capture CO_2. The reformer tubes are located into the fuel reactor or in a fluidized bed heat exchanger connected to the chemical-looping system, a procedure which provides very favourable conditions for the required heat transmission.

For H_2 production, the SR-CLC unit is integrated with water-gas shift (WGS) and pressure swing adsorption (PSA) units. In the WGS reactor the hydrogen production is maximized by conversion of CO by the WGS reaction. Next, the hydrogen is separated from the other components in a pressure swing adsorption unit (PSA). After water removal, the PSA unit is able to recover between 75 to greater than 90% of the overall hydrogen in the syngas. The unrecovered H_2 and the rest of the gases are sent to the FR. A typical PSA tail gas composition is 50-55 vol.% CO_2, 24-26 vol.% H_2, 15-20 vol.% CH_4, 0-2 vol.% CO and 0-5 vol.% H_2O depending on the operating parameters [6].

In the SR-CLC process, the PSA tail gas is used as a fuel gas in the fuel reactor of the CLC system. A net heat balance showed that the combustion of the PSA tail gas can provide the sufficient heat needed for the reforming reaction of methane [7]. To increase the heating value of the PSA tail gas, natural gas can be added.

Rydén and Lyngfelt [4] showed a preliminary reactor design in order to demonstrate the feasibility of the SR-CLC process. They concluded that the reactor dimensions seem to be reasonable, and the SR-CLC process has potential to achieve better selectivity towards H_2 than conventional SR plants due to low reactor temperatures and favorable heat-transfer conditions. However, very little research has been conducted about the performance of a CLC system using PSA tail gas as fuel. Ortiz et al. [7] conducted a study on the behavior of an iron waste from aluminium manufacture, as an oxygen carrier for the SR-CLC process. The iron waste oxygen carrier was used in a 500 W_{th} CLC unit to burn different kind of gas fuels such as PSA tail gas, syngas and CH_4. The OC showed enough high oxygen transport capacity and reactivity to fully convert syngas at 880 ºC. However, lower conversion of the fuel was observed with methane containing fuels. An estimated solids inventory of 1600 kg/MW_{th} would be necessary to fully convert the PSA off-gas to CO_2 and H_2O using this OC.

An important key in the development of the SR-CLC technology is the selection of an appropriate OC. Because of its low cost and environmental compatibility, Fe-based OC are considered an attractive option for CLC application. These OC have shown enough reactivity at atmospheric [8-11] and pressurized conditions [12], and they can fully convert methane into CO_2 and H_2O. Other chemical characteristics are advantageous for the use of Fe-based oxygen carriers: low tendency to carbon deposition [12] and no risk of sulphide or sulphate formation at any concentration or operating temperature when sulphur containing fuels are used [13].

Iron compounds need special attention due to their different final oxidation states during reduction reaction (Fe_2O_3-Fe_3O_4-FeO-Fe). The oxygen transport capacity, R_{OC}, was defined as the mass fraction of oxygen that can be used in the oxygen transfer. The reduction of Fe_2O_3 can be stopped in one of the above products, and consequently, the

value of R_{OC} will be very different depending on the reaction considered, being for the reaction Fe_2O_3/Fe three times higher than for the reaction Fe_2O_3/FeO and for this reaction three times higher than for the reaction Fe_2O_3/Fe_3O_4. The stable iron species are dependent on the reducing gas composition and temperature. However, only the transformation from hematite to magnetite (Fe_2O_3-Fe_3O_4) may be applicable for industrial CLC systems. Further reduction to wustite (FeO) or Fe would produce a high decrease in the CO_2 purity obtained in the fuel reactor because of the increase in the equilibrium concentrations of CO and H_2 [13]. When alumina or titania are present in the particles, $FeO{\cdot}Al_2O_3$ or $FeTiO_3$ can be formed as reduced compound –which corresponds to Fe^{+2}- in order to fully convert the gas to CO_2 and H_2O [14-16]. Thus, the oxygen transport capacity is increased regarding the Fe_2O_3/Fe_3O_4 system. Besides these thermodynamic limitations, some authors have found agglomeration problems associated with the reaction from wustite to magnetite [17-18]

To develop a suitable oxygen carrier, synthetic materials, low-cost minerals, ores and waste products have been evaluated. There are several studies working with synthetic Fe-based oxygen carriers using different supports, (sepiolite, SiO_2, TiO_2 ZrO_2 and Al_2O_3), different preparation methods, and metal contents [14-16,19]. As it was pointed out above, the use of alumina as support has a positive effect on the oxygen transport capacity of the oxygen-carrier if $FeO{\cdot}Al_2O_3$ is formed [15]. Thus, Abad et al [19] used an oxygen-carrier of 60 wt. % of Fe_2O_3 and Al_2O_3 as support prepared by freeze granulation in 300W_{th} continuous unit. Tests using natural gas or syngas as fuel were carried out at temperatures from 800 to 950ºC for a total of 40 h in combustion conditions, without any sign of deactivation, agglomeration, carbon deposition, and very little attrition. The combustion efficiency of syngas was high, about 99% for all

experimental conditions. However for methane combustion, efficiencies ranged up to 94%.

It is well-known that the preparation method and the metal content can affect to the properties of the OC [20]. Usually, impregnated particles have shown higher reactivity with CH_4, CO and H_2 than particles prepared by mechanical mixing [21].

The purpose of this study was to evaluate the behaviour of an impregnated Fe-based oxygen carrier supported on Al_2O_3 in the combustion of a PSA tail gas for the SR-CLC process. Reactivity with different reducing gases, such as CO, H_2 and CH_4 will be measured in TGA. Batch fluidized bed characterization in order to analyze the product gas distribution and the fluidization behaviour of the oxygen carrier will be also analyzed. Experiments in a CLC continuous unit will be carried out using a simulated PSA off-gas stream as fuel. For comparison purposes, the behavior of this material using methane as fuel will be also studied. The effect on the combustion efficiency of different operating conditions, such as fuel composition, oxygen carrier to fuel ratio and fuel reactor temperature will be determined in the continuous unit. Finally, a characterization of fresh and after-used particles will be also performed to investigate the possible changes undergone the oxygen carrier after continuous operation.

2. Experimental section

2.1. Oxygen carrier material

The behaviour of an impregnated oxygen carrier based on Fe was analyzed in this work. Commercial γ-Al_2O_3 (Puralox NWa-155, Sasol Germany GmbH) particles of 0.1-0.32 mm, with density of 1.3 g/cm^3 and porosity of 55.4 % were selected as support.

A modification of the incipient impregnation method was carried out by using a hot iron nitrate solution in order to increase the solubility of the nitrate. The OC was prepared by

impregnation of the support heated at 80ºC in a planetary mixer using a saturated iron nitrate solution at 60-80ºC (3.8 M). The OC was prepared by addition of a hot volume of the solution corresponding to the total pore volume of the support particles. The aqueous solution was slowly added to the alumina particles, with thorough stirring at hot temperature. The desired active phase loading was achieved by applying two successive impregnations followed by calcination at 550ºC, in air atmosphere for 30 min. Finally the particles were sintered for 1 hour at 950 ºC.

The main physical and chemical properties of the OC are shown in Table 1. As mentioned above, the oxygen transport capacity, R_{OC}, for the Fe-based oxygen carriers can be different depending on the final oxidation state reached during the reduction reaction. In this work the R_{OC} value was calculated assuming that reduction was stopped in the form of $FeO{\cdot}Al_2O_3$. As it can be seen in Table 1, the active Fe_2O_3 content of the OC is 15.2 wt. % corresponding to an oxygen transport capacity of 1.5 %. The mechanical strength has an adequate value for fluidization operation and the porosity and BET area values are high. The support was transformed from γ-Al_2O_3 to the more stable phase α-Al_2O_3 during the calcination stage.

2.2 Oxygen carrier characterization

Several techniques have been used to characterize physically and chemically the fresh and after-used oxygen carrier particles. The Fe_2O_3 active content for the CLC process was determined by complete reduction of the sample with hydrogen in TGA at 950ºC. The force needed to fracture a particle was determined using a Shimpo FGN-5X crushing strength apparatus. The mechanical strength was taken as the average value of at least 20 measurements. The real density of the particles was measured with a Micromeritics AccuPyc II 1340 helium picnometer. The surface area of the oxygen

carrier was determined by the Brunauer-Emmett-Teller (BET) method by adsorption/desorption of nitrogen at 77 K in a Micromeritics ASAP-2020 (Micromeritics Instruments Inc.), whereas the pore volume was measured by Hg intrusion in a Quantachrome PoreMaster 33. The identification of crystalline chemical species was carried out by powder X-ray diffractometer Bruker AXS graphite monochromator. Some oxygen carrier particles were also analyzed in a scanning electron microscope (SEM) ISI DS-130 coupled to an ultra thin window PGT Prism detector for energy-dispersive X-ray (EDX) analysis.

2.3. Reactivity tests in TGA

The reactivity of the oxygen carrier was determined in a TGA, CI electronics type, described elsewhere [8]. For the experiments, the oxygen carrier was loaded in a platinum basket and heated to the set operating temperature in air atmosphere. After weight stabilization, the experiment was started by exposing the oxygen carrier to alternating reducing and oxidizing conditions. To avoid mixing of combustible gas and air, nitrogen was introduced for two min after each reducing and oxidizing period.

The reactivity of the oxygen carrier was determined with different reducing gases: CH_4, CO and H_2 at different temperatures (830, 880 and 950 ºC). The gas composition was 15 vol.% of the reducing gas. In the experiments with CH_4, 20 vol. % H_2O was introduced to avoid carbon formation by methane decomposition. Steam was incorporated to the gas stream by bubbling through a water containing saturator at the selected temperature to reach the desired water concentration. Similarly, 20 vol. % CO_2 was introduced together with CO to avoid carbon formation by the carbon gasification reaction. In all cases, nitrogen was used to balance. For oxidation reaction, 100% air was used as reacting gas.

The conversion of solids for the reduction reaction was calculated as:

$$X_r = \frac{m_{ox} - m}{R_{OC} m_{ox}} \quad (1)$$

m_{ox} being the mass of the fully oxidized solids, m the instantaneous mass of the sample and R_{OC} the oxygen transport capacity of solids for the transformation between Fe_2O_3 and $FeO{\cdot}Al_2O_3$, given by Table 1. The conversion for the oxidation reaction was calculated as $X_o = 1 - X_r$.

2.4. Fluidized bed reactor

Several reduction-oxidation multicycles were carried out in a batch fluidized bed reactor to know the gas product distribution during reaction and the fluidization behaviour of the carrier with respect to attrition and agglomeration phenomena.

Figure 2 shows the experimental setup used for testing the oxygen carrier. It consisted of a system for gas feeding, a fluidized bed (FB) reactor, a two ways system to recover the solids elutriated from the FB, and a gas analysis system. The gas feeding system had different mass flow controllers for different gases and water. The FB reactor of 54 mm I.D. and 500 mm height, with a preheating zone just under the distributor, was fed with 200-300 g of oxygen carrier with a particle size of 0.1-0.3 mm and the entire system was inside an electrically heated furnace. The reactor had two connected pressure taps in order to measure the differential pressure drop in the bed. Agglomeration problems, causing defluidization of the bed, could be detected by a sharp decrease in the bed pressure drop during operation. Two hot filters located downstream from the FB recovered the solids elutriated from the bed during the successive reduction-oxidation cycles. Different gas analyzers measured continuously the gas composition at each time. The CO, CO_2, H_2O, and CH_4 gas concentrations were measured in two infrared

analyzers (FTIR and NDIR), the O_2 concentration was measured in a paramagnetic analyzer, and the H_2 concentration was measured by gas conductivity.

The tests were carried out at 950ºC with an inlet superficial gas velocity into the reactor of 10 cm/s. The composition of the gas was 25 vol.% CH_4 in N_2 during reduction and 15 vol.% O_2 in N_2 during oxidation. The reduction periods were varied between 60 and 300 s. The oxidation periods necessary for complete oxidation varied between 600 and 1200 s. To avoid mixing of CH_4 and O_2, N_2 was introduced for two minutes after each reducing and oxidizing period.

The conversion of the oxygen carriers as a function of time during the reduction and oxidation periods were calculated from the gas outlet concentrations by the equations:

Reduction

$$X_{red} = \int_{t_0}^{t_{red}} \frac{Q_{out}}{n_0 P_{tot}} \left(2P_{CO_2,out} + P_{CO,out} + P_{H_2O,out}\right) dt \tag{2}$$

$$Q_{out} = Q_{in}\left(\frac{P_{N_2 in}}{P_{N_2 out}}\right) = Q_{in}\left(\frac{P_{N_2,in}}{(1 - P_{CH_4,out} - P_{CO_2,out} - P_{CO,out} - P_{H_2,out} - P_{H_2O,out})}\right) \tag{3}$$

Oxidation

$$X_{oxi} = \int_{t_0}^{t_{oxi}} \frac{2Q_{out}}{n_0 P_{tot}} \left(\frac{Q_{in}}{Q_{out}} P_{O_2,in} - P_{O_2,out} - 1/2 P_{CO,out} - P_{CO_2,out}\right) dt \tag{4}$$

$$Q_{out} = \frac{Q_{in}(1 - P_{O_2,in})}{(1 - P_{CO_2,out} - P_{CO,out} - P_{O_2,out})} \tag{5}$$

where X_i is the conversion of the oxygen carrier, Q_{in} is the molar flow of the gas coming into the reactor, Q_{out} is the molar flow of the gas leaving the reactor, P_{tot} is the total pressure, $P_{i,in}$ is the partial pressure of gas i incoming to the reactor, $P_{i,out}$ is the partial

pressure of gas i exiting the reactor, n_0 are the moles of oxygen which can be removed from fully oxidized oxygen carrier, and t is the time. The last terms in equation 4 take into account the formation of CO and CO_2 during the oxidation period due to the oxidation of C coming from the decomposition of CH_4 in the reduction period.

2.5. ICB-CSIC-g1 facility

Figure 3 shows a schematic diagram of the continuous atmospheric CLC facility used in this work, which was designed and built at Instituto of Carboquimica (CSIC). The pilot plant was basically composed of two interconnected fluidized-bed reactors –the air and fuel reactors–, a riser for solids transport from the air reactor (AR) to the fuel reactor (FR), a solid valve to control the solids flow rate fed to the fuel reactor, a loop seal and a cyclone. This design allowed the variation and control of the solid circulation flow rate between both reactors.

The FR (1) consisted of a bubbling fluidized bed (0.052 m i.d.) with a bed height of 0.1 m. In this reactor the oxygen carrier particles are reduced by the fuel. Reduced oxygen carrier particles overflowed into the AR (3) through a U-shaped fluidized bed loop seal (2), to avoid gas mixing between fuel and air. The oxidation of the carrier took place at the AR, which consisted of a bubbling fluidized bed (0.05 m i.d.) with a bed height of 0.1 m, followed by a riser (4) of 0.02 m i.d. and 1 m height. The regeneration of the oxygen carrier happened in the dense bed part of the AR allowing residence times high enough for the complete oxidation of the reduced carrier. Secondary air could be introduced at the top of the bubbling bed to help particle entrainment. N_2 and unreacted O_2 left the AR passing through a high-efficiency cyclone (5) and a filter (9) before the stack. The oxidized solid particles recovered by the cyclone were sent to a solids reservoir setting the oxygen carrier ready to start a new cycle. In addition, these

particles avoid the leakage of gas between the FR and the riser. The regenerated oxygen carrier particles returned to the FR by gravity from the solids reservoir through a solids valve (7) which controlled the solids circulation flow-rate entering the FR. A diverting solids valve (6) located below the cyclone allowed the measurement of the solids flow rates at any time. Fine particles produced by fragmentation/attrition in the plant were recovered in the filters that were placed downstream of the FR and AR. The gas outlet streams of the FR and AR were drawn to respective on-line gas analyzers to get continuous data of the gas composition. CH_4, CO, CO_2 were measured at the fuel reactor outlet via an NDIR analyzer (Maihak S710) together with H_2 using a thermal conductivity analyzer (Maihak S710). At the outlet of air reactor, CO and CO_2 were measured by an NDIR analyzer (Siemens/Ultramat 22P), and O_2 by a paramagnetic analyzer (Siemens/Oxymat 5E).

The total solids inventory in the system was about 1.2 kg of solid material. The temperature in the air reactor was always kept constant at about 950 ±15ºC. The inlet flow of fuel was 170 Nl h^{-1}, which corresponds to an inlet gas velocity in the fuel reactor of 10 cm s^{-1}. The inlet air flow in the AR was 720 Nl h^{-1} as primary air, (46 cm s^{-1} at 880ºC), and 150 NL h^{-1} as secondary air. Nitrogen was used to fluidize the bottom loop seal (37.5 Nl h^{1}).

Table 2 shows a summary of the different operating conditions used in the tests. Two different fuels were used during the experimental work: a simulated PSA off-gas stream and CH_4. The composition of the simulated PSA off-gas fed to the FR was 12 % of CH_4, 18 % of CO, 25 % of H_2 and 45 % of CO_2 [22]. In most of experiments, the PSA off-gas was diluted with nitrogen. Under all operating conditions, the ratio of the constituent gases of the PSA off-gas, i.e. CH_4, H_2, CO, CO_2 was maintained constant.

The oxygen carrier-to-fuel ratio (ϕ) was defined by Eq. (6), as:

$$\phi = \frac{F_{Fe_2O_3}}{bF_{Fuel}} \tag{6}$$

$F_{Fe_2O_3}$ being the molar flow rate of the iron oxide and F_{Fuel} is the inlet molar flow rate of the fuel in the FR. The parameter b is the stoichiometric coefficient of the fuel gas mixture, calculated in Eq. (7) as:

$$b = \frac{4x_{CH_4} + x_{CO} + x_{H_2}}{x_{CH_4} + x_{CO} + x_{H_2}} \tag{7}$$

Thus, the oxygen carrier-to-fuel ratio (ϕ) was defined as the ratio between the oxygen supplied and the oxygen needed to stoichiometrically react with the fuel flow. A value of the ϕ ratio equal to unity means that the oxygen supplied by the solids is exactly the stoichiometric oxygen to fully convert the fuel gas to CO_2 and H_2O.

To analyze the effect of the ϕ ratio, experiments PSA-1 to PSA-4 (Table 2) were carried out varying the flow of the PSA off-gas, but maintaining roughly constant the solids circulation flow-rate at about 13 kg h^{-1}. To maintain the total flow of gas entering to the fuel reactor, the corresponding flow of nitrogen was added in every case. When the flow of PSA off-gas was varied, the air to fuel ratio, the solids inventory per MW_{th} (m^*_{FR}) and the gas concentration were varied simultaneously.

To analyze the effect of FR temperature on combustion efficiency the experiments were carried out at two different FR temperature, 830 and 880ºC. Experiments PSA-1 to PSA-4 were performed at 830ºC, and experiments PSA-5 to PSA-7 at 880ºC.

Additional experiments were carried out using methane as fuel gas at 830 ºC (M-1 to M-5) or 880 ºC (M-6 to M-9). Similarly to the experiments using PSA off-gas, different fuel gas concentrations were selected to vary the ϕ ratio.

To evaluate the behaviour of the oxygen carrier during the combustion tests, the combustion efficiency η_c, defined in Eq. (8), was used as a key parameter. The combustion efficiency (η_c) was defined as the ratio of the oxygen consumed by the gas leaving the FR to that consumed by the gas when the fuel is completely burnt to CO_2 and H_2O. So, the ratio gives an idea about how the CLC operation is close or far from the full combustion of the fuel, i.e. η_c = 100%.

$$\eta_c = \frac{\left(2x_{CO_2} + x_{CO} + x_{H_2O}\right)_{out} F_{out} - (2x_{CO_2} + x_{CO})_{in} F_{in}}{\left(4x_{CH_4} + x_{CO} + x_{H_2}\right)_{in} F_{in}} 100 \quad (8)$$

F_{in} being the molar flow of the inlet gas stream, F_{out} the molar flow of the outlet gas stream, and x_i the molar fraction of the gas in the inlet or outlet gas stream.

3.Results and discussion.

3.1. Reactivity in TGA

The oxygen carrier must have sufficient reactivity to be able to fully convert the fuel gas, and the deactivation of the oxygen carrier during operation in a CLC system should be minimized. Reactivity tests of fresh and after-used oxygen carrier particles were carried out in the TGA. Figure 4 a) shows the reduction and oxidation conversions versus time curves obtained using H_2, CO and CH_4 as reacting gases, and air for the oxidation at 830ºC. In all cases the conversion was calculated assuming that Fe_2O_3 was reduced to the form Fe^{+2}. This assumption was confirmed by the results obtained by the

XRD patterns, as it can be seen in Table 1, which shows that the final reduced form in the experiments carried out using CH_4 was only the form $FeO{\cdot}Al_2O_3$. However, conversions higher than one were measured using H_2 and CO as reacting gases. It must be pointed out that using H_2 or CO different reduction states can be reached depending on the ratios H_2O/H_2/ or CO_2CO/ used [15]. In the TGA conditions used in this work, reduction up to Fe could be reached. XRD patterns, shown in Table 1, confirmed these results.

As it can be seen in Figure 4 a), the oxygen carrier exhibited very fast reduction and oxidation rates with all reacting gases. The reactivities obtained with the different reducing gases had no important differences between them. The similar reactivities found with this OC disagree with the ones obtained by Abad et al. [11,19] who determined that the reactivity of a synthetic iron-based oxygen carrier was higher using H_2 or CO than the one obtained with CH_4 as a reducing gas. Also Leion et al. [14] and Adánez et al. [23] observed the same behaviour with ilmenite, a natural mineral mainly composed by iron and titanium and Ortiz et al [7] using an iron waste material. This fact revealed the improved CH_4 reactivity of this Fe-based impregnated OC compared to other Fe-based materials found in the literature.

The effect of temperature on the reactivity of the OC was evaluated using the different fuel gases at 830, 880 and 950 °C. Figure 4 b) shows the reactivities obtained at 950 °C with H_2, CO and CH_4 as reacting gases. The highest reactivity was measured at 950ºC and the lowest at 830ºC. Small differences were observed between reactivities of the carrier at 830 and 880ºC for the different gases, but considerable differences were observed when the temperature was increased up to 950 ºC, specially for H_2 and CO. Thus, temperatures about 950 ºC would be desirable to have a high reactivity OC with CH_4, H_2 and CO, gases that are all part of the PSA-offgas.

3.2. Batch fluidized bed reactor

Several reduction-oxidation cycles with CH_4 as reducing gas were performed in the batch fluidized bed to investigate the gas product distribution, the variation of the carrier reactivity with the number of cycles and the behaviour of the carrier particles with respect to the attrition and agglomeration phenomena.

To analyze the gas product distribution the reactions happening with different contribution during the oxygen carrier reduction-oxidation with CH_4, CO and H_2 must be considered. Thus, the following reactions can take place in the reactor during the oxygen carrier reduction period:

Oxygen carrier reduction

$$4\ Fe_2O_3 + 8\ Al_2O_3 + CH_4 \leftrightarrow 8\ FeO{\cdot}Al_2O_3 + CO_2 + 2\ H_2O \quad \text{(R1)}$$

$$Fe_2O_3 + 2\ Al_2O_3 + H_2 \leftrightarrow 2\ FeO{\cdot}Al_2O_3 + H_2O \quad \text{(R2)}$$

$$Fe_2O_3 + 2\ Al_2O_3 + CO \leftrightarrow 2\ FeO{\cdot}Al_2O_3 + CO_2 \quad \text{(R3)}$$

Partial oxidation

$$Fe_2O_3 + 2\ Al_2O_3 + CH_4 \leftrightarrow 2\ FeO{\cdot}Al_2O_3 + CO + 2\ H_2 \quad \text{(R4)}$$

Methane decomposition

$$CH_4 \leftrightarrow C + 2\ H_2 \quad \text{(R5)}$$

Carbon gasification

$$C + H_2O \leftrightarrow CO + H_2 \quad \text{(R6)}$$

$$C + CO_2 \leftrightarrow 2\ CO \quad \text{(R7)}$$

Water gas shift

$$CO + H_2O \leftrightarrow CO_2 + H_2 \quad \text{(R8)}$$

And during the oxygen carrier oxidation:

Oxygen carrier oxidation

$$4\,FeO + O_2 \leftrightarrow 2\,Fe_2O_3 \quad \text{(R9)}$$

Carbon combustion

$$C + O_2 \leftrightarrow CO_2 \quad \text{(R10)}$$

$$C + \tfrac{1}{2}\,O_2 \leftrightarrow CO \quad \text{(R11)}$$

Figure 5 shows the outlet product gas distribution for the 6th cycle working with the Fe-based oxygen carrier at 950ºC using CH_4 as fuel in the batch fluidized bed reactor. The back-mixing in the system, which was illustrated by the transient changes in gas concentration during the first seconds of reaction, was considered in order to obtain the actual concentration of the gases in the bed. The correction was done using a deconvolution method to take into account for the distribution of the residence time of the gas in the system [24]. As it can be seen, there was a first period of approximately one minute of full conversion of CH_4, where CO_2 and/or H_2O were formed just immediately after introduction of the reducing gas to the reactor, and no CH_4 leaves the reactor. After that, as a consequence of the oxygen depletion, the rate of oxygen transference decreases. As a result, CO_2 and H_2O concentrations begin to decrease and the CH_4, CO and H_2 concentrations starts to increase because there is not enough oxygen available to fully convert CH_4 into CO_2 and H_2O, and the partial oxidation of methane takes place. In the oxidation period, CO_2 and CO were formed by the combustion of C generated in the reduction period by CH_4 decomposition. Figure 5 also shows the solid conversion, X_s, as a function of the reducing time. In all cases the conversion was calculated assuming that Fe_2O_3 was reduced to the form $FeO{\cdot}Al_2O_3$. This assumption was confirmed by the results obtained by the XRD patterns, as it can be seen in Table 1, which shows that the final reduced form was only the form $FeO{\cdot}Al_2O_3$. The conversion increases very quickly as a result of the loss of oxygen from the carrier. The first section corresponds to the period of full conversion of fuel

into CO_2 and water. Similar results were found during the whole batch experiments indicating that the OC maintains its reactivity during cycling operation.

The multi-cycle tests carried out in the batch fluidized bed reactor were useful to determine the fluidization behaviour of the oxygen carrier with respect to the agglomeration phenomena. As it was pointed out, some authors have found agglomeration problems working with Fe-bases OCs [17-18]. However, although a high degree of conversion was reached in the batch fluidized reactor the carrier did not show any agglomeration behaviour during operation. These experiments were also used to determine the attrition rate of the carrier. The attrition rate was obtained from the particles elutriated from the FB reactor retained in a heated filter. The Fe-based oxygen carrier showed low attrition rates. The weight loss was 0.075 %/h during the first two hours and after that decreased to a stable value of 0.02 %/h.

3.3. Test in ICB-CSIC-g1 facility

A total of about 46 h at hot conditions, of which 40 corresponded to combustion conditions were carried out in the facility using the impregnated Fe-based oxygen carrier. The effect of oxygen carrier-to-fuel ratio, the temperature of the fuel reactor and the fuel composition on the combustion efficiency, η_c, was analyzed. PSA off-gas and methane were used as fuel gases during the experimental tests.

The gas product concentrations of the fuel and air reactors were measured by on line analyzers. These gas concentrations were used to make carbon, hydrogen and oxygen mass balances over the whole reactor system. For better comparison, the results are presented in N_2 free basis and/or dry basis.

As an example, Figure 6 shows the temperature profiles and the gas product distribution in the FR and AR using PSA off-gas as fuel and operating conditions corresponding to

test PSA-5. The outlet gas concentrations and the temperatures were uniform during the whole combustion time. Mass balances were found to be accurate by using the measurements of the analyzers from the AR and FR. The combustion efficiency reached in this operation condition was around 99 %, without any CH_4, H_2 or CO measured at the outlet of the FR.

A suitable oxygen carrier should not promote the formation of solid carbon in the FR. Carbon deposited on particles could be transported to the AR, where combustion with oxygen will happen. In this case, CO_2 will be emitted from the AR, reducing the carbon capture efficiency of the chemical-looping combustor. Carbon deposition on particles could happen in the FR by methane decomposition (R5) and the carbon gasification reaction (R7). In the CLC continuous unit, carbon formation was evaluated by measuring CO and CO_2 concentrations at the outlet of the AR. As there was not gas leakage from the FR to AR, any carbon containing gas present in the AR outlet should come from solid carbon following the oxygen carrier particles. These gases were never detected in the AR in any test. Thus, no losses in CO_2 capture were produced by carbon transfer to the AR, reaching 100 % CO_2 capture in the process.

3.3.1. Effect of the oxygen carrier-to-fuel ratio

The effect of oxygen carrier-to-fuel ratio on the combustion efficiency of the PSA off-gas was studied varying the fuel concentration in the gas fed to the fuel reactor. All of the other experimental conditions were maintained constant. Figure 7 (a) shows the effect of ϕ on the combustion efficiency working with PSA-offgas as fuel, at 830 ºC. These experiments correspond to tests PSA-1 to PSA-4. An increase in the ϕ value, produces an increase in the combustion efficiency, due to the higher availability of

oxygen in the FR. It can be observed that working at 830ºC it can be obtained a combustion efficiency of 100% at ϕ values equal or higher than 4.

Figure 8 shows the effect of ϕ on the gas product concentration measured at the outlet of the FR working with PSA-offgas as fuel, with a FR temperature of 830ºC. It can be observed how an increase in the oxygen carrier to fuel ratio produced a decrease in the H_2, CO and CH_4 concentrations, due to the higher amount of oxygen in the reactor, and therefore the increase of the contribution of the reduction reactions (reactions (R1)-(R3)). As it can be seen, similar outlet concentrations of each gas were measured, indicating similar oxygen carrier reactivity with each gas. This fact agrees with the results obtained in TGA, where it was found that the reactivity of the carrier with CO, H_2 and CH_4 was very similar.

3.3.2. Effect of the FR temperature

The effect of the FR temperature on the combustion efficiency was tested at 880ºC with PSA-offgas. These experiments correspond to tests PSA-5 to PSA-7. Figure 7 (a) shows the experimental results obtained. It can be observed that an increase in the FR temperature produced an important increase in the combustion efficiencies as a consequence of higher oxygen carrier reactivity, as it could seen in the results obtained with TGA. Therefore, full conversion of the PSA off-gas fuel can be reached with this OC working at 880ºC and ϕ values higher than 2.

Figure 8 also shows the effect of ϕ on the gas product distribution at the outlet of the FR working with PSA-offgas as fuel at different temperatures. It can be observed an important decrease in the unconverted gases when the FR temperature was increased to 880ºC. So it can be concluded that at 880 °C the oxygen carrier was enough reactive to

fully convert CH_4, CO and H_2 coming from a PSA off gas stream at values of ϕ higher than 1.5.

3.3.3. Effect of the fuel composition

The effect of the fuel gas composition was studied using methane. Figure 7 (b) shows the effect of ϕ on the combustion efficiency working with CH_4 as fuel, at 830 ºC (tests M-1 to M-5) and at 880ºC (tests M-6 to M-9). As it can be seen comparing figures 7 (a) and 7 (b) the combustion efficiency variation with ϕ was very similar independently of the fuel gas used, although PSA-offgas has 43% of $CO+H_2$, gases that react faster than methane [7,11,14,15,22] with Fe-based OC. Moreover, Figure 7 (b) shows the effect of the FR temperature on the combustion efficiency when CH_4 was used. An important increase in the combustion efficiency was observed. Similar results to those obtained with PSA-offgas independently of the FR temperature were found. So, it can be said that the fuel composition has low effect on the combustion efficiency using this OC and full conversion of CH_4 to CO_2 and H_2O can be obtained at $\phi > 1.5$.

Figure 9 show the effect of the oxygen carrier to fuel ratio on the gas product distribution measured at the outlet of the FR working with CH_4 as fuel, at 830 and 880ºC respectively. A decrease in the value of ϕ produces a decrease in the combustion efficiency due to an increase in the amount of unconverted gases at the outlet of the fuel reactor, i.e. CH_4, H_2 and CO. However, H_2 and CO concentrations were very low. During the combustion of methane side reactions can occur, like the partial oxidation of methane (reaction R4), and the reforming reaction and water-gas shift equilibrium, which could generate variable amounts of CO and H_2. Thermodynamic calculations were performed to check if the outgoing gases were in WGS equilibrium. The only unconverted fuel at equilibrium should be CO and H_2. As the main unconverted gas at

the exit of the FR was methane, it can be concluded that CH_4 reforming and partial oxidation was slow and equilibrium in the gas phase was not reached in the experimental tests.

The use of a specific OC has important implications for a CLC system. The reactivity of the solids determines the solids inventory in the system. From the results obtained in this work, to reach full conversion of the fuel (both PSA-offgas or CH_4) at 830ºC ϕ values equal or higher than 4 were necessary. As it can be seen in Table 2, this corresponds to a solids inventory around 1100 kg/MW_{th}. The amount of solids necessary for complete conversion of gas decreased with increasing the FR temperature. At 880ºC, the solids inventory necessary to reach full conversion of fuel was around 500 kg/MW_{th} . These values are considerably lower than the ones obtained by Ortiz et al [7], who estimated that the solids inventory needed to fully convert the PSA off-gas to CO_2 and H_2O, using a Fe-based waste material as oxygen carrier would be around 1600 kg/MW_{th} at 880ºC. Indeed, the values obtained in this work are much lower than the ones estimated by Abad et al [19], who calculated a solids inventory of 1200 kg/MW_{th} for a methane conversion of 99 % at 850ºC using a synthetic Fe-based OC. Moreover, the differences in the amount of Fe metal necessary from these OC are also remarkable. On the basis of the amount of Fe in the solid particles per MW, the Fe inventory for the impregnated OC of this work was 10 times lower than the corresponding to the freeze granulated OC [19]. A Fe inventory of only 50 kg/MW_{th} should be necessary to fully convert methane or PSA-offgas in a CLC system working at 880ºC and using the impregnated Fe_2O_3/Al_2O_3 OC of this work.

3.3.4. Oxygen carrier behaviour

It is important that the OC can survive for long period of time in a CLC system. A total of 46 h at hot conditions, of which 40 h corresponded to combustion conditions, were carried out in continuous operation. A batch of particles of 1.2 kg was used without replacement or adding new material. During operation, different solid samples were taken from the cyclones and filters to study the variation in their physical and chemical properties with time. It must be pointed out that during the whole operation time, the oxygen carrier particles never showed agglomeration or defluidization problems.

Attrition and fragmentation of particles was also analyzed during the process. Particles elutriated from the fluidized bed reactors during operation were recovered in the cyclones and filters and weighted to determine the attrition rate. It was assumed as attrition those particles of size under 40 μm. Figure 10 shows the evolution with time of the attrition rate of the oxygen carrier during the whole operation in the continuous unit. The attrition rate was high during the first hours as a consequence of the rounding effects on the irregularities of the particles and because of the fines stuck to the particles during their preparation. However, the attrition rate after 20 h of operation stabilized at approximately 0.08 wt.%/h which remains roughly constant up to the 46 hours of operation. This attrition rate corresponds to a particle lifetime of 1250 h. Although the attrition rate measured during operation in the ICB-CSIC-g1 facility was higher than the one obtained in the batch fluidized bed reactor, higher gas velocities in the air reactor and the existence of a riser and a cyclone in the continuous unit must be taken into account.

The reactivity of the particles in the CLC unit seemed to be maintained constant for the whole tests. To confirm this fact, the reactivity of the used oxygen carrier particles at different operation times was analyzed by TGA. A gas composed of 15 vol.% CH_4 and

20 vol.% H_2O for the reduction and air for the oxidation were used at 950 ºC. Figure 4b) shows the conversion versus time for the reduction and oxidation reaction of the used particles. As can be seen, the reduction and oxidation reactivities of the oxygen carrier were similar to the fresh ones after its operation in the CLC continuous unit. The Fe_2O_3 content of the used particles was also determined by complete reduction of the sample with hydrogen in TGA. The iron content in the oxygen carrier remains constant, maintaining the oxygen transport capacity of the material at 1.5 %, as it was shown in Table 1.

The evolution of the textural and structural properties of the oxygen carrier was studied by different techniques. Table 1 shows the main properties of this batch of used oxygen carrier particles and were compared to those of fresh particles. A slightly decrease of the mechanical strength of the particles, from 1.5 N to 1.2 N was observed after operation at high temperatures. An oxygen carrier with high attrition and/or fragmentation of particles can be a problem during operation in CLC. Nevertheless, the attrition rate measured in the CLC system was stable and moderate.

The real density of the used particles presented a very slight increase. The carrier porosity slightly decreased and the BET surface area remains at low values after operation.

The powder XRD patterns showed the presence of hematite in the samples extracted from the air reactor which indicates that full oxidation of the oxygen carrier was performed. Iron aluminate, $FeO{\cdot}Al_2O_3$, was found in the reduced samples taken from the fuel reactor. No other iron phases than hematite and $FeO{\cdot}Al_2O_3$ were found in the different samples analyzed during operation coming from the fuel and air reactor. The fine particles recovered in the AR filters were composed of Fe_2O_3 and Al_2O_3 in the same proportion as in the fresh OC.

Some oxygen carrier particles were also analyzed by SEM-EDX. Figure 11 shows SEM images of carrier particles, fresh and after operation. As shown in Figures 11(a) and (b), the oxygen carrier particles exhibited an irregular shape and the general appearance of the used particles was similar to the fresh particles. No changes in the surface texture and the solid structure of the used particles were detected, compared to fresh particles; see Figures 11(c) and (d). The iron distribution inside the particles was analyzed by EDX in some particles embedded in resin epoxy, cut, and polished. It was found a uniform distribution of iron through the particles and there was not evidence of redistribution or migration during the redox cycles after comparing Figures 11(g) and (h). Moreover, no signs of agglomeration were observed in SEM pictures of used particles, agreeing with the avoidance of defluidization problems in the CLC continuous unit.

4. Conclusions

A synthetic Fe-based oxygen carrier was used in a continuous CLC unit to burn a PSA tail gas in order to evaluate the SR-CLC process. The oxygen carrier was made by incipient hot impregnation using Al_2O_3 as support and was first characterized by TGA and batch fluidized bed reactor to determinate the CH_4, CO and H_2 reactivity and the fluidization behaviour of the oxygen carrier.

Continuous operation in the CLC facility was performed during 46 h using a simulated PSA off-gas and methane as fuels. The effect of oxygen carrier-to-fuel ratio and the reactor temperature on the combustion efficiency was analyzed.

TGA reactivity showed that the oxygen carrier exhibited very fast reduction and oxidation rates with all reacting gases. This fact revealed the improved CH_4 reactivity of

this Fe-based impregnated OC compared to other Fe-based materials found in the literature.

An oxygen carrier to fuel ratio > 1.5 in the continuous CLC unit was needed to reach full combustion efficiencies working with a PSA-offgas at 880ºC. It was found an important effect of the temperature of FR on the combustion efficiency. The needed oxygen carrier to fuel ratio at 830ºC increased up to 4 to reach full combustion efficiency. However, the fuel composition had low effect on the combustion efficiency. The combustion efficiency variation with ϕ was very similar for methane and PSA-offgas.

The oxygen carrier did not show any agglomeration, carbon deposition or defluidization problems after more than 46 h of continuous operation in the CLC facility. The attrition rate measured was stable and adequate for operation in a fluidized-bed reactor.

The solids inventory needed to reach full combustion of the fuel was around 500 kg/MW_{th} for PSA-offgas or CH_4 at 880ºC, which corresponds to a Fe inventory of 50 kg/MW_{th}. These metal inventories are much lower than those found with other Fe-based materials, both natural and synthetic. These results show the significant positive effect of using alumina as support on impregnated Fe-based OC. Therefore, the Fe_2O_3/Al_2O_3 oxygen carrier prepared by impregnation is suitable for burning a PSA tail gas for the H_2 production with CO_2 capture in the SR-CLC process.

Acknowledgments

This work was partially supported by the Spanish Ministry of Science and Innovation (MICINN) (CTQ2007-64400). M. Ortiz thanks Diputación General de Aragón for the F.P.I. fellowship. M.A. Pans thanks MICINN for the FPI fellowship.

References

[1] IPCC Special Report on Carbon Dioxide Capture and Storage. 2005. http://www.ipcc.ch.

[2] J.R. Rostrup-Nielsen, Catal. Today. 18 (1993) 305-324.

[3] M. Rydén, A. Lyngfelt, A. Schulman, L.F. de Diego, J. Adanez, M. Ortiz, T. Pröll, J. Bolhàr-Nordenkampf, P. Kolbitsch, in: Carbon dioxide capture for storage in deep geological formations - Results from the CO_2 capture project. Ed. L. I. Eide, UK, CPL Press, 2009, vol. 3, ch. 14.

[4] M.Rydén, A.Lyngfelt, Int. J. Hydrogen Energy. 31 (2006) 1271-1283.

[5] H.R. Kerr, in: Carbon Dioxide Capture for Storage in Deep Geologic Formations – Results from the CO_2 Capture Project. Ed. D. Thomas, S. Benson, Elsevier Ltd., Oxford, UK, 2005, vol. 1, ch. 38.

[6] S. Reddy, S, Vyas. Energy Procedia. 1 (2009) 149-154.

[7] M. Ortiz, P. Gayán, L. F. de Diego, F. García-Labiano, A. Abad, M. A. Pans, J. Adánez, J. Power Sources. 196 (2011) 4370-4381.

[8] J. Adanez, L.F. de Diego, F. Garcia-Labiano, P. Gayan, A. Abad, J.M. Palacios, Energy Fuels. 18 (2004) 371-377.

[9] T. Mattisson, M. Johansson, A. Lyngfelt, Energy Fuels. 18 (2004) 628-637.

[10] M. Johansson, T. Mattisson, A. Lyngfelt, Ind. Eng. Chem. Res. 43 (2004) 6978-6987.

[11] A. Abad, J. Adanez, F. Garcia-Labiano, L.F. de Diego, P. Gayan, J. Celaya, Chem. Eng. Sci. 62 (2007) 533-549.

[12] P. Cho, T. Mattisson, A. Lyngfelt, Ind. Eng. Chem. Res. 44 (2005) 668-76.

[13] E. Jerndal, T. Mattisson, A. Lyngfelt, Chem. Eng. Res. Des. 84 (2006) 795-806.

[14] H. Leion, A. Lyngfelt, M. Johansson, E. Jerndal, T. Mattisson, Chem. Eng. Res. Des. 86 (2008) 1017-1026.

[15] A. Abad, F. Garcia-Labiano, L.F. de Diego, P. Gayan, A. Adanez, Energy Fuels. 21 (2007) 1843-1853.

[16] B. Corbella, J.M. Palacios, Fuel. 86 (2007) 113-122.

[17] P. Cho, T. Mattisson, A. Lyngfelt, Ind. Eng. Chem. Res. 45 (3) (2006) 968-977.

[18] M. Ryden, E. Cleverstam, M. Johansson, T. Mattisson, AIChE J. 56 (8) (2010) 2211-2220.

[19] A. Abad, T. Mattisson, A. Lyngfelt, M. Johansson, Fuel. 86 (2007) 1021-1035.

[20] P.Gayan, L. F. de Diego, F. Garcia-Labiano, J. Adanez, A. Abad, C. Dueso, Fuel. 87 (2008) 2641-2650.

[21] L.F. de Diego, F. Garcia-Labiano, J. Adanez, P. Gayan, A. Abad, B. M. Corbella, J.M. Palacios, Fuel. 83 (2004) 1749-1757.

[22] Final report. CACHET project (FP VI-019972).

[23] J. Adánez, A. Cuadrat, A. Abad, P. Gayán, L. F. de Diego, F. García-Labiano, Energy Fuels. 24 (2010) 1402-1413.

[24] O. Levenspiel in: Chemical Reaction Engineering, John Willey and Sons, New York, 1981.

Captions for the Figures

Figure 1. Schematic diagram of (a) CLC and (b) SR-CLC

Figure 2. Experimental setup used for multicycle tests.

Figure 3. Schematic diagram of the ICB-CSIC-g1 facility.

Figure 4. Conversion vs. time curves of the oxygen carrier working with different reacting gases: H_2, CO and CH_4 at a) 830ºC, fresh OC particles, and b) 950ºC, fresh and after used (46 h CLC unit) OC particles.

Figure 5. Product gas distribution in dry basis during reduction and subsequent oxidation for the 6th cycle with CH_4 at 950ºC. H_2O concentration as measured in an FTIR analyzer.

Figure 6. Temperature and gas product distribution at the outlet of FR and AR during a typical experiment. Experimental test PSA-5: T_{FR} = 880ºC, T_{AR} = 950ºC, PSA off-gas = 100 vol %, f_S = 13.4 kg h^{-1}, ϕ = 1.9.

Figure 7. Effect of oxygen carrier to fuel ratio on the combustion efficiency working with PSA-offgas (a): 880ºC (-□-) , 830ºC (-◊-) and with CH_4 (b): 880ºC (--■--), 830ºC (--♦--).

Figure 8. Effect of oxygen carrier to fuel ratio on the composition of outlet gas working with PSA-offgas at 830ºC: (-■-) CH_4, (--▲--) CO, (··●··) H_2, and at 880 ºC: (-□-) CH_4, (--Δ--) CO, (··○··) H_2.

Figure 9. Effect of oxygen carrier to fuel ratio on the composition of outlet gas working with CH_4 as fuel at 830ºC: (-■-) CH_4, (--▲--) CO, (··●··) H_2, and at 880 ºC : (-□-) CH_4, (--Δ--) CO, (··○··) H_2.

Figure 10. Attrition rate versus time measured in the CLC unit.

Figure 11. SEM-EDX images of the oxygen carrier particles both fresh (left) and after 46 h of operation in the CLC unit (right); (a) and (b) SE (secondary electrons) image of the particles; (c) and (d) BSE (back-scattering electrons) photograph of cross section of the particles; (e) and (f) BSE image of a cross section of a particle; (g) and (h) EDX line profile of Fe in a cross section of a particle.

Table 1. Main characteristics of the oxygen carrier.

				fresh	**after used** [a]
Fe_2O_3 [b] (wt. %)				15.2	15.2
Oxygen transport capacity [c] (%)				1.5	1.5
Crushing strength (N)				1.5	1.2
Real density (g/cm^3)				3.95	4.12
Porosity (%)				50.5	47.1
Specific surface area, BET (m^2/g)				39.1	9.3
XRD	fresh			α-Al_2O_3, Fe_2O_3	
	used	TGA	oxidation with air		α-Al_2O_3, Fe_2O_3
			reduction with CH_4		α-Al_2O_3, $FeO{\cdot}Al_2O_3$
			reduction with H_2		α-Al_2O_3, Fe
		Batch	oxidation with air		α-Al_2O_3, Fe_2O_3
			reduction with CH_4		α-Al_2O_3, $FeO{\cdot}Al_2O_3$
		CLC	particles from AR		α-Al_2O_3, Fe_2O_3
			particles from FR		α-Al_2O_3, $FeO{\cdot}Al_2O_3$
			particles from AR filter		α-Al_2O_3, Fe_2O_3

[a] 46 h CLC unit
[b] Determined by TGA
[c] $R_{OC} = (m_{ox}-m_{red})/m_{ox}$

Table 2. Operating conditions and main data for the experiments carried out in the ICB-CSIC-g1 facility.

Test	**Fuel gas** [a] (vol. %)	$\mathbf{T_{FR}}$	$\mathbf{f_s}$ (kg/h)	ϕ	**Power** (W_{th})	m^*_{FR} (kg/MW_{th})
PSA						
PSA-1	100.0	830	13.5	1.9	438	471
PSA-2	72.1	830	13.5	2.6	316	653
PSA-3	57.5	830	13.5	3.2	252	819
PSA-4	45.9	830	13.5	4.0	180	1146
PSA-5	100.0	880	13.4	1.9	438	471
PSA-6	72.1	880	13.4	2.6	316	653
PSA-7	57.5	880	13.4	3.2	252	819
CH_4						
M-1	35.0	830	13.5	1.2	592	348
M-2	25.0	830	13.5	1.6	423	487
M-3	19.9	830	13.5	2.0	337	612
M-4	15.5	830	13.5	2.5	262	786
M-5	10.0	830	13.5	4.0	169	1219
M-6	36.8	880	13.9	1.1	623	331
M-7	35.0	880	13.9	1.2	592	348
M-8	29.4	880	13.9	1.5	498	414
M-9	14.5	880	13.9	3.0	246	839

[(a)] N_2 to balance

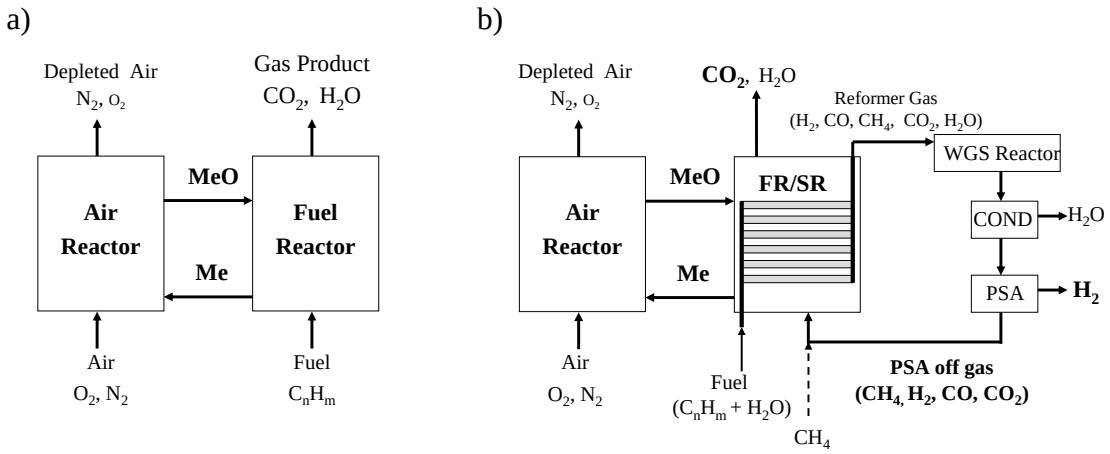

Figure 1. Schematic diagram of (a) CLC and (b) SR-CLC

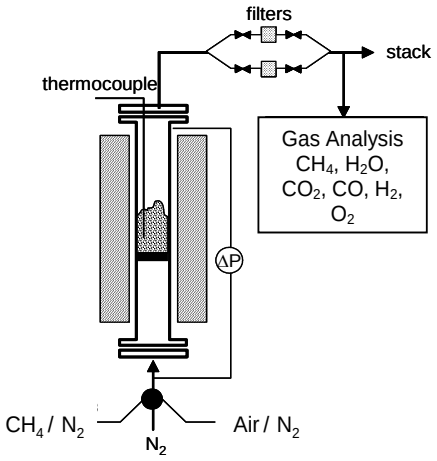

Figure 2. Experimental setup used for multicycle tests.

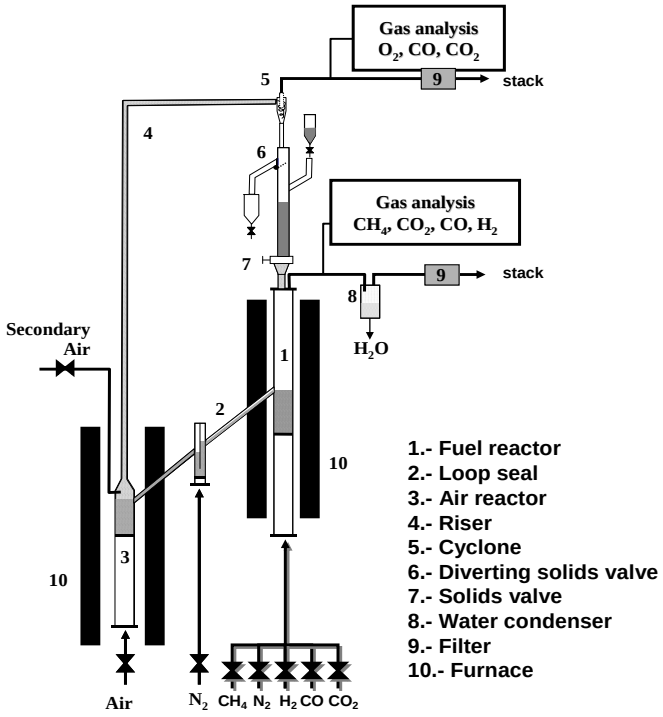

Figure 3. Schematic diagram of the ICB-CSIC-g1 facility.

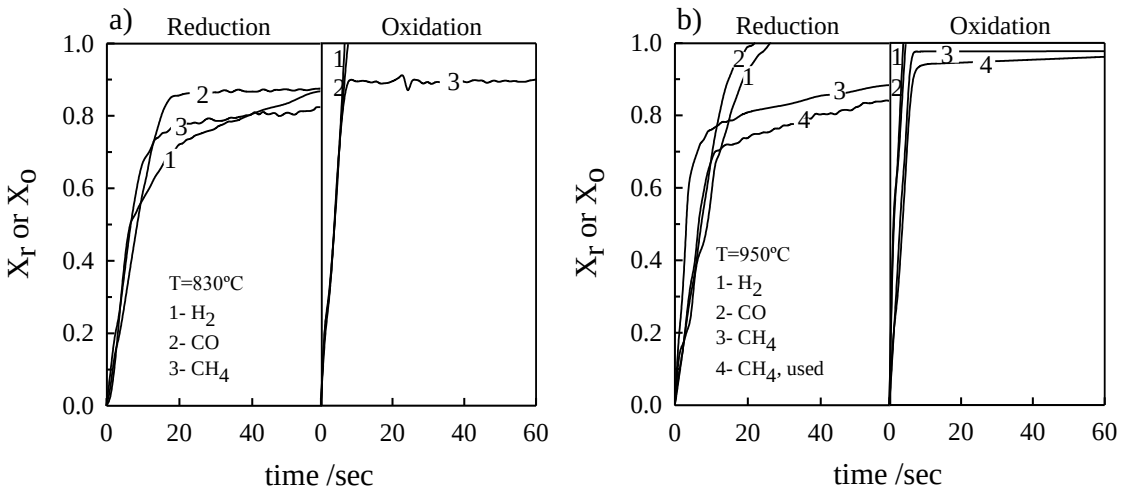

Figure 4. Conversion vs. time curves of the oxygen carrier working with different reacting gases: H_2, CO and CH_4 at a) 830ºC, fresh OC particles, and b) 950ºC, fresh and after used (46 h CLC unit) OC particles.

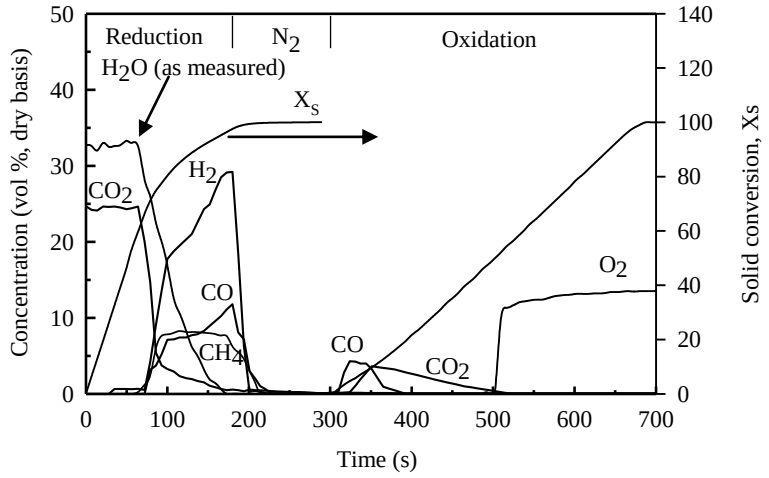

Figure 5. Product gas distribution in dry basis during reduction and subsequent oxidation for the 6th cycle with CH_4 at 950ºC. H_2O concentration as measured in an FTIR analyzer.

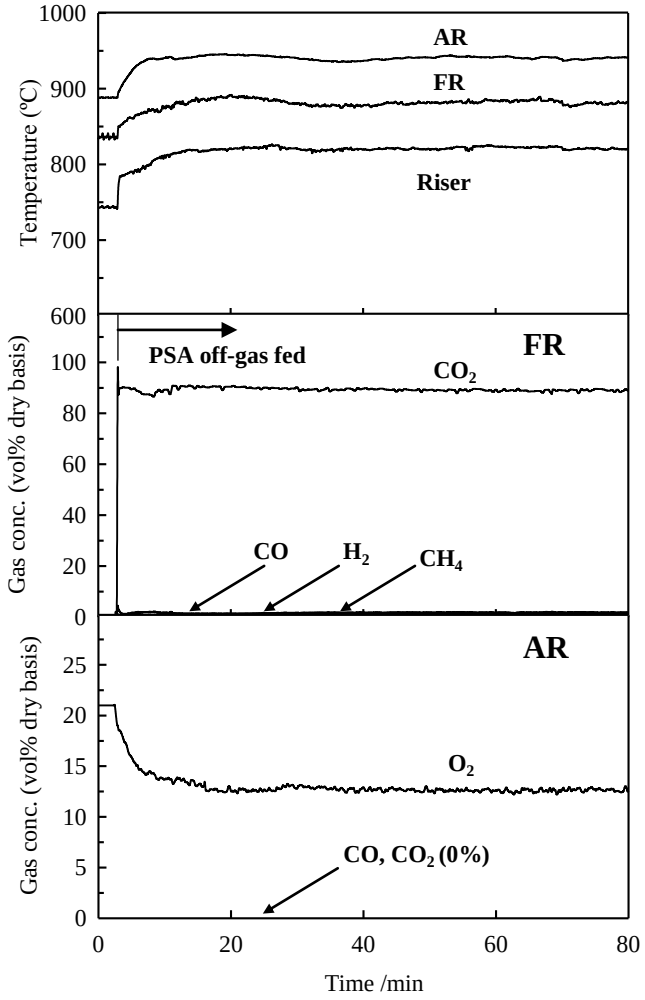

Figure 6. Temperature and gas product distribution at the outlet of FR and AR during a typical experiment. Experimental test PSA-5: T_{FR} = 880ºC, T_{AR} = 950ºC, PSA off-gas = 100 vol %, f_S = 13.4 kg h^{-1}, ϕ = 1.9.

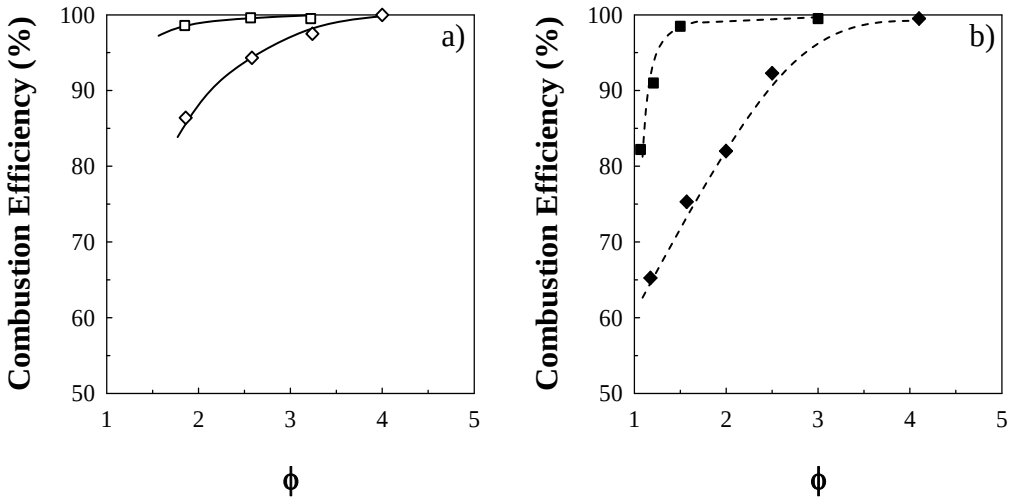

Figure 7. Effect of oxygen carrier to fuel ratio on the combustion efficiency working with PSA-offgas (a): 880ºC (-□-) , 830ºC (-◊-) and with CH_4 (b): 880ºC (--■--), 830ºC (--♦--).

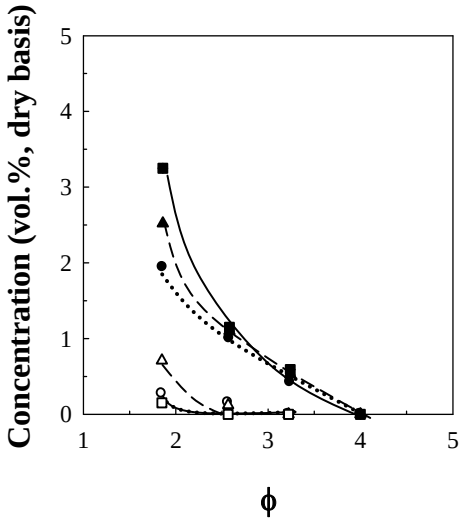

Figure 8. Effect of oxygen carrier to fuel ratio on the composition of outlet gas working with PSA-offgas at 830ºC: (-■-) CH_4, (--▲--) CO, (··●··) H_2, and at 880 ºC: (-□-) CH_4, (--Δ--) CO, (··○··) H_2.

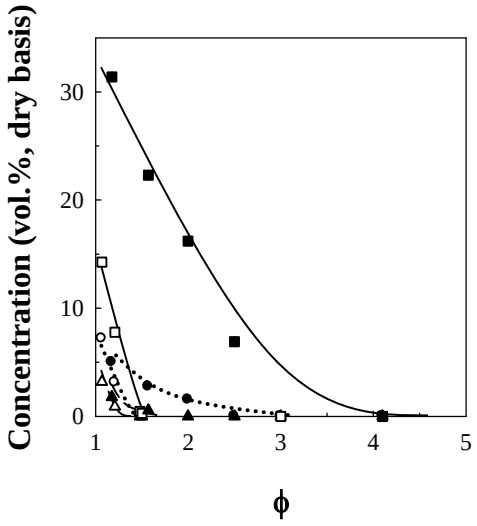

Figure 9. Effect of oxygen carrier to fuel ratio on the composition of outlet gas working with CH_4 as fuel at 830ºC: (-■-) CH_4, (--▲--) CO, (··●··) H_2, and at 880 ºC : (-□-) CH_4, (--Δ--) CO, (··○··) H_2.

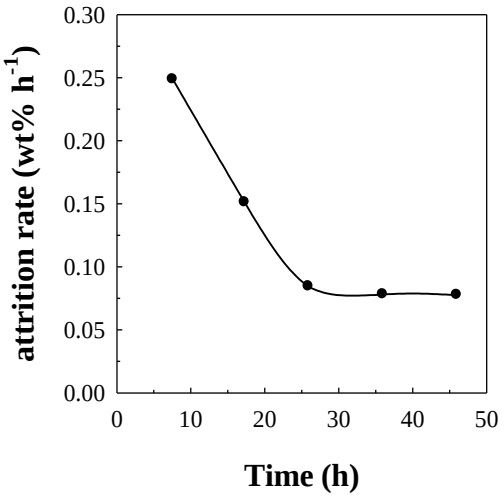

Figure 10. Attrition rate versus time measured in the CLC unit.

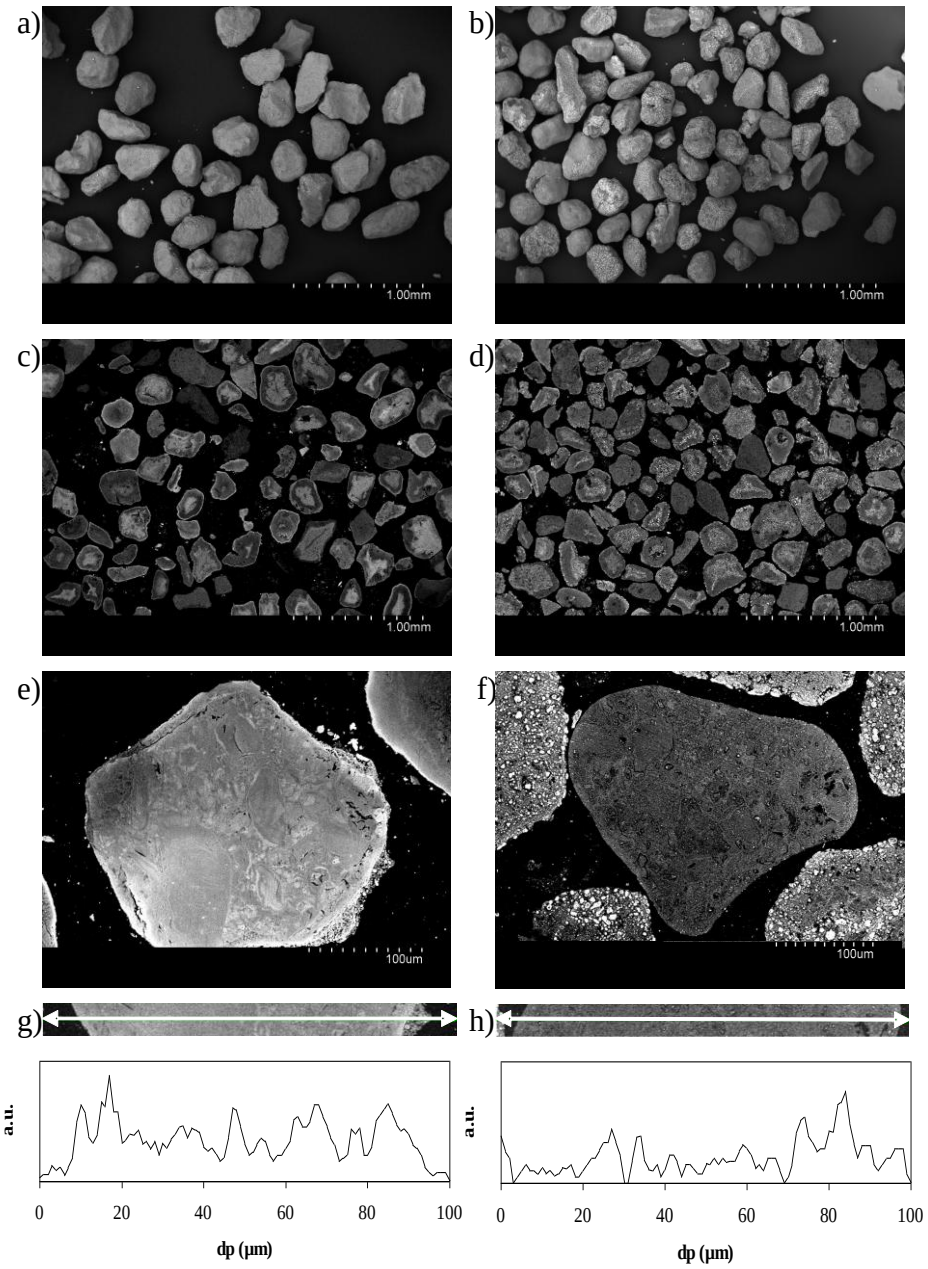

Figure 11. SEM-EDX images of the oxygen carrier particles both fresh (left) and after 46 h of operation in the CLC unit (right); (a) and (b) SE (secondary electrons) image of the particles; (c) and (d) BSE (back-scattering electrons) photograph of cross section of the particles; (e) and (f) BSE image of a cross section of a particle; (g) and (h) EDX line profile of Fe in a cross section of a particle.